Acta Cryst E
CRYSTALLOGRAPHIC COMMUNICATIONS
ISSN 2056-9890

Synthesis, crystal structure, Hirshfeld surface analysis, MEP study and molecular docking of *N*-{3-[(4-methoxyphenyl)carbamoyl]phenyl}-3-nitrobenzamide as a promising inhibitor of hfXa

Rodolfo Moreno-Fuquen,[a]* Mario Hurtado-Angulo,[a] Kevin Arango-Daraviña,[a] Gavin Bain[b] and Alan R. Kennedy[b]

[a]Grupo de Cristalografía, Departamento de Química, Universidad del Valle, A.A 25360 Santiago de Cali, Colombia, and [b]WestCHEM. Department of Pure and Applied Chemistry, University of Strathclyde, 295 Cathedral Street, Glasgow G1XL, Scotland. *Correspondence e-mail: rodolfo.moreno@correounivalle.edu.co

Received 22 July 2020
Accepted 13 October 2020

Edited by G. Diaz de Delgado, Universidad de Los Andes, Venezuela

Keywords: crystal structure; Hirshfeld surfaces; molecular electrostatic potential; molecular docking.

CCDC reference: 2016019

Supporting information: this article has supporting information at journals.iucr.org/e

The title compound, $C_{21}H_{17}N_3O_5$, consists of three rings, *A*, *B* and *C*, linked by amide bonds with the benzene rings *A* and *C* being inclined to the mean plane of the central benzene ring *B* by 2.99 (18) and 4.57 (18)°, respectively. In the crystal, molecules are linked *via* N—H···O and C—H···O hydrogen bonds, forming fused $R_2^2(18)$, $R_4^3(30)$, $R_4^4(38)$ rings running along $[\bar{1}0\bar{1}]$ and $R_3^3(37)$ and $R_3^3(15)$ rings along [001]. Hirshfeld analysis was undertaken to study the intermolecular contacts in the crystal, showing that the most significant contacts are H···O/O···H (30.5%), H···C/C···H (28.2%) and H···H (29.0%). Two zones with positive (50.98 and 42.92 kcal mol^{-1}) potentials and two zones with negative (−42.22 and −34.63 kcal mol^{-1}) potentials promote the N—H···O interactions in the crystal. An evaluation of the molecular coupling of the title compound and the protein with enzymatic properties known as human coagulation factor Xa (hfXa) showed the potential for coupling in three arrangements with a similar minimum binding energy, which differs by approximately 3 kcal mol^{-1} from the value for the molecule Apixaban, which was used as a positive control inhibitor. This suggests the title compound exhibits inhibitory activity.

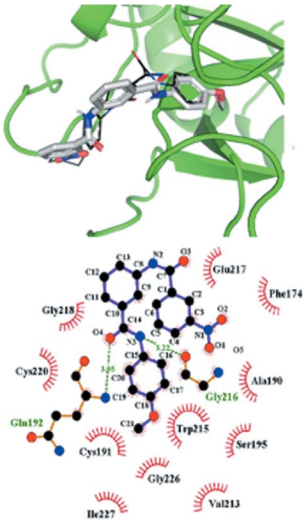

1. Chemical context

The synthesis of new compounds derived from aminobenzamides has generated a growing interest in the search for molecular systems that can have different physical, chemical or biological properties. Some aminobenzamide derivatives present high efficiencies in their non-linear optical properties (Prasad *et al.*, 2011). Exceptional insecticidal activity against lepidopterous insects has been shown by some anthranilic diamides (Lahm *et al.*, 2005) and benzene dicarboxamide derivatives (Tohnishi *et al.*, 2005; Lahm *et al.*, 2007). Other substituted benzamides are used as medications for patients with schizophrenia (Racagni *et al.*, 2004). Some benzamide compounds are used in the area of neurology for their powerful neuroprotective effects (Hirata *et al.*, 2018). Other diamide compounds analogous to the product obtained in this work have been tested as potential options for antithrombotic treatments by acting as direct inhibitors of coagulation factor Xa (Xing *et al.*, 2018; Lee *et al.*, 2017). This study was undertaken with the aim of providing new compounds with possible pharmaceutical applications. The results of the synthesis,

OPEN ACCESS

crystal-structure determination by single-crystal X-ray diffraction, supramolecular analysis and an evaluation of molecular coupling on human factor Xa of the title compound, (I), a new diamide derived from 3-aminobenzamide, is presented here.

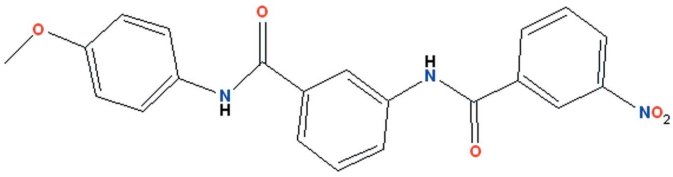

2. Structural commentary

In the title compound, Fig. 1, the mean planes of rings *A* (C1–C6; r.m.s deviation = 0.0127 Å) and *C* (C15–C20; r.m.s deviation = 0.0086 Å) form dihedral angles of of 2.99 (18) and 4.57 (18)°, respectively, with the mean plane of the central ring *B* (C8–C13; r.m.s deviation = 0.0072 Å). In turn, the amide groups C8/N2/C7(O3)/C1 (r.m.s deviation = 0.0081 Å) and C15/N3/C14(O4)/C10 (r.m.s deviation = 0.0101 Å), which link the rings, are inclined by 37.72 (15) and 29.35 (16)°, respectively, to ring *B*. The nitro group forms an angle of 5.3 (2)° with ring *A* while the methoxy group is approximately coplanar with ring *C*, forming an angle of 1.1 (5)°. The molecule is formed by three main planes resulting from the planes that form the rings with the *B* ring resembling a fallen step between *A* and *C*. All bond lengths (Allen *et al.*, 1987) and bond angles are within normal ranges.

3. Supramolecular features

The crystalline packing in compound (I) is mainly regulated by the presence of N—H···O and C—H···O hydrogen bonds. The N2—H2*N*···O4^{i} and N3—H3*N*···O3^{ii} interactions [symmetry codes: (i) $-x+1, y+\frac{1}{2}, -z+1$; (ii) $-x, y+\frac{1}{2}, -z+1$] form fused $R_2^2(18)$, $R_4^3(30)$ and $R_4^4(38)$ rings (Etter, 1990) running along [$\bar{1}0\bar{1}$] (see Table 1 and Fig. 2*a*). In turn, playing the role of complementary interactions in crystal growth, other C—H···O-type interactions [C19—H19···O1^{iv} and C21—H21*C*···O1^{v}; symmetry codes: (iv) $x-1, y, z+1$; (v) $-x+1, y-\frac{1}{2}, -z+1$] link the molecules at their ends, ensuring their stability in the growth process. Together with the N—H···O interactions, they contribute to the formation of additional fused $R_3^3(37)$ and $R_3^3(15)$ rings, which run along [001] (see Table 1, Fig. 2*b*). Weak C21—H21*B*···*Cg*1 interactions occur, where *Cg*1 is the centroid of the C1–C6 benzene ring, with a H21*B*···*Cg*1 distance of 2.83 Å.

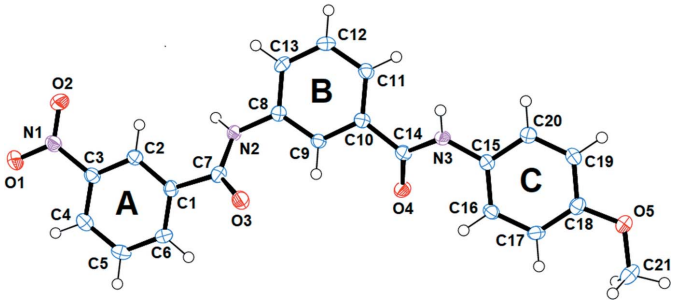

Figure 1
The molecular structure of (I), showing the atom labeling and displacement ellipsoids drawn at the 50% probability level.

Table 1
Hydrogen-bond geometry (Å, °).

D—H···*A*	*D*—H	H···*A*	*D*···*A*	*D*—H···*A*
N2—H2*N*···O4^{i}	0.88	2.09	2.908 (4)	155
N3—H3*N*···O3^{ii}	0.88	2.21	3.056 (4)	163
C5—H5···O2^{iii}	0.95	2.28	3.093 (5)	143
C19—H19···O1^{iv}	0.95	2.44	3.365 (5)	164
C21—H21*C*···O1^{v}	0.98	2.64	3.490 (5)	145

Symmetry codes: (i) $-x+1, y+\frac{1}{2}, -z+1$; (ii) $-x, y+\frac{1}{2}, -z+1$; (iii) $x, y-1, z$; (iv) $x-1, y, z+1$; (v) $-x+1, y-\frac{1}{2}, -z+1$.

4. Hirshfeld surface analysis

Intermolecular interactions, including hydrogen-bond interactions, are essential in reinforcing the stability of the supramolecular structure. This behavior can be analyzed through the study of Hirshfeld surfaces (HS) using the *CrystalExplorer* program (Spackman & Jayatilaka, 2009), which allows the visualization of the interactions within the crystal structure, including N···H and C···H interactions. To examine in depth the strength and capacity of hydrogen bonds and other intermolecular contacts, one of the Hirshfeld surface analysis tools, the normalized contact distance, d_{norm}, has been used (Turner *et al.*, 2017). The results show that the most important

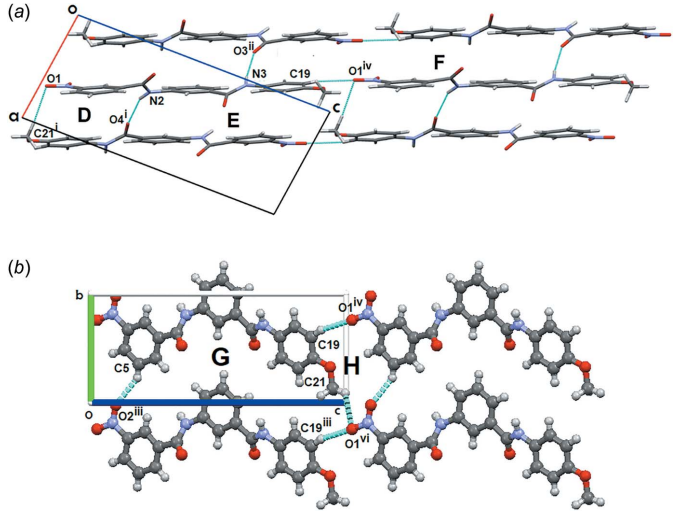

Figure 2
(*a*) Partial crystal structure of (I), showing the formation of **D** = $R_2^2(18)$, ***E*** = $R_4^3(30)$ and **F** = $R_4^4(38)$ fused rings running along [$\bar{1}0\bar{1}$] and (*b*) **G** = $R_3^3(37)$ and **H** = $R_3^3(15)$ fused rings. These fused rings run along [001]. Symmetry code: (vi) $x-1, y-1, z+1$.

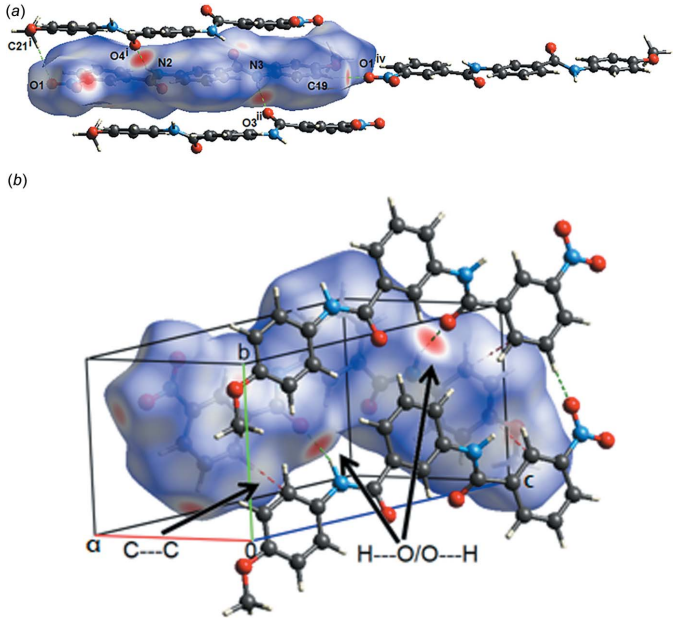

Figure 3
(*a*) A view of the Hirshfeld surface of (I) mapped over d_{norm} emphasizing the N—H···O and C—H···O intermolecular interactions and (*b*) showing the H···O/O···H and C···C (π–π) interactions. Symmetry codes: (i) $-x+1, y+\frac{1}{2}, -z+1$; (ii) $-x, y+\frac{1}{2}, -z+1$; (iii) $x-1, y, z+1$.

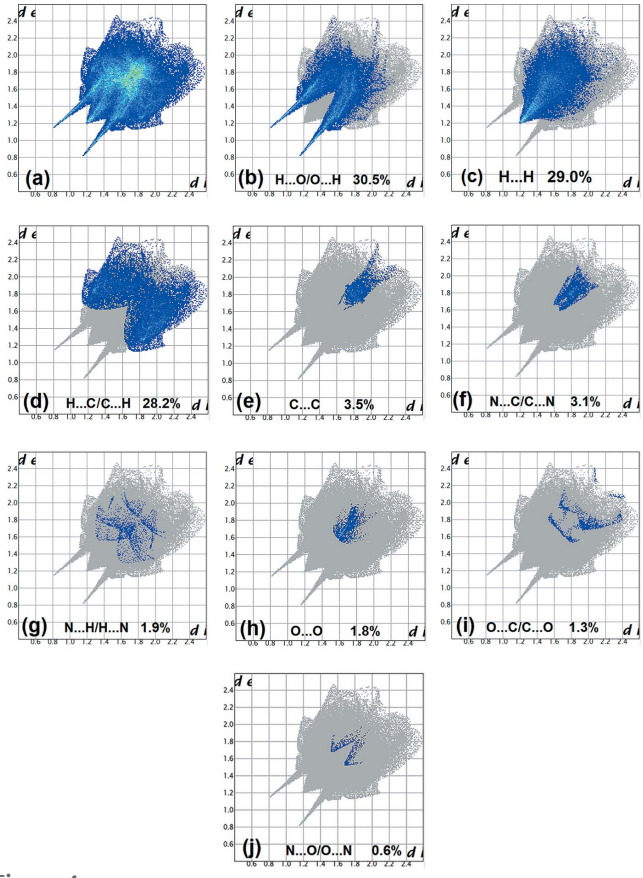

Figure 4
Two-dimensional fingerprints plots for the title compound, showing (*a*) all interactions, (*b*) H···O/O···H, (*c*) H···H, (*d*) H···C/C···H, (*e*) C···C, (*f*) N···C/C···N, (*g*) H···N/N···H, (*h*) O···O, (*i*) O···C/C···O, and (*j*) N···O/O···N interactions. The d_i and d_e values are the closest internal and external distances (in Å) of given points on the Hirshfeld surface.

contributions to the crystal packing are due to the N—H···O and C—H···O hydrogen bonds. This is evidenced by the more intense red spots on the HS for (I) (see Fig. 3*a*,*b*). The overall two-dimensional fingerprint plot (Fig. 4*a*), and those delineated into by H···O/O···H, H···H, H···C/C···H, C···C, N···C/C···N, H···N/N···H, O···O, O···C/C···O, and N···O/O···N contacts are illustrated in Fig. 4*b*–*j*, respectively, together with their relative contributions to the Hirshfeld surface. The most important interaction corresponds to H···O/O···H contributing 30.5% to the overall crystal packing, as shown in Fig. 4*b*. The pair of spikes in the fingerprint plot have a symmetrical distribution of high-density points with the tip at $d_e + d_i = 1.98$ Å. The H···H interactions, shown in Fig. 4*c*, contribute 29.0% to the total crystal packing and appear as widely dispersed points of high density due to the large hydrogen-atom content of the molecule with the rounded tip at $d_e + d_i = 1.20$ Å. The presence of C—H···π interactions is shown as a pair of characteristic wings on the fingerprint plot (Fig. 4*d*), delineated into H···C/C···H contacts (28.2% contribution to the HS) having the tip at $d_e + d_i = 2.84$ Å. These results reveal the importance of H-atom contacts in establishing the packing. The large number of H···H, H···C/C···H and H···O/O···H interactions suggest that van der Waals interactions and hydrogen bonding play major roles in the crystal packing (Hathwar *et al.*, 2015).

5. Molecular Electrostatic Potential (MEP)

A study of the molecular electrostatic potential (MEP) of (I) using the *Gauss09W* (Frisch *et al.*, 2009) and *Gauss View 5.0* programs, at the DFT/B3LYP/6-31G (d, p) level of theory, to obtain a qualitative analysis and the *Multiwfn 3.6* program for a quantitative analysis (Lu & Chen, 2012) of the surface was undertaken. On the potential surface, marked in dark blue, positive regions of low electron density that can suffer nucleophilic attacks in a chemical reaction or can have interactions with nucleophiles in the process of crystalline growth are shown (see Fig. 5). Two zones show positive potentials of 50.98 and 42.92 kcal mol^{-1} in regions that follow the directions of the N—H bonds above and below the plane through the

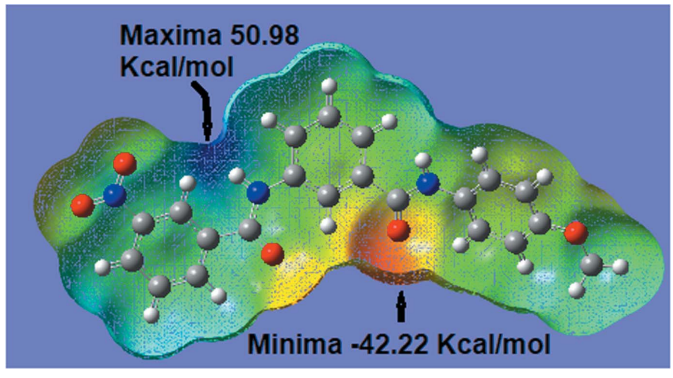

Figure 5
Three-dimensional representation of the electrostatic potential around a molecule of (I).

Table 2
Molecular coupling calculations (kcal mol^{-1}) for the active hfXa site, the title compound, and the Apixaban molecule.

Compound	Bond energy[a]	No. of hydrogen bonds[b]	Hydrogen-bonding interaction residues[b]	van der Waals interaction residues[b]
(I)	−7.7	1	Gly218	Trp215, Cys191, Ser195, Gln192, Cys220, Gly218, Ala190, Gly216, Gly 226, Asp189, Val213, Phe174, Glu217, Glu 146
Apixaban[c]	−10.7	3	Gly216, Gln192, Glu146	Cys220, Tyr99, Glu97, Phe174, Thr98, Val213, Trp215, Gly226, Cys191, Asp189, Ser195, Ile227, Ala190, Gly218, Arg143

Notes: (*a*) The binding energy indicates the affinity and binding capacity for the active site of the enzyme protein fXa; (*b*) The number of hydrogen bonds and all amino acid residues involved in the enzyme-inhibitor complex were determined using *AutoDock 4.2.6* (Trott & Olson, 2010); (*c*) The Apixaban molecule was used as a positive control ligand for the active site.

Table 3
Equivalent poses of compound (I) in the active hfXa site, as a result of molecular coupling calculations (kcal mol^{-1}).

Compound	Bond energy[a]	No. of hydrogen bonds[b]	Hydrogen-bonding interaction residues[b]	van der Waals interaction residues[b]
(I) (pose 1)	−7.7	1	Gly218	Trp215, Cys191, Ser195, Gln192, Cys220, Gly218, Ala190, Gly216, Gly 226, Asp189, Val213, Phe174, Glu217, Glu 146
(I) (pose 2)	−7.6	1	Gly192	Phe174, Tyr99, Val213, Gly226, Trp215, Ser195, Asp189, Ala190, Gly218, Gly216, Cys191, Gln192, Ile 227, Lys96
(I) (pose 3)	−7.4	2	Gly 216, Gln192	Cys220, Glu217, Phe174, Val213, Gly226, Cys191, Ser195, Ala190, Trp215, Gly218, Ile227

Notes: (*a*) The binding energy indicates the affinity and binding capacity for the active site of the enzyme protein fXa; (*b*) The number of hydrogen bonds and all amino acid residues involved in the enzyme-inhibitor complex were determined using *AutoDock 4.2.6* (Trott & Olson, 2010); (*c*) The Apixaban molecule was used as a positive control ligand for the active site.

rings of the molecule and which promote the formation of the N2—H2*N*···O4^{i} and N3—H3*N*···O3^{ii} hydrogen bonds throughout the crystal. In turn, other areas with high density, being close to the carbonyl oxygen atoms and shown in a reddish color, show values of −42.22 and −34.63 kcal mol^{-1}. Thus, in the first stage of crystal formation, these low and high electronic density regions are intertwined to promote the formation of rings and chains of molecules along the crystal. The other areas with lower values in the regions will be accommodated to enable the formation of other weaker bonds, C5—H5···O2^{iii}, C19—H19···1^{iv} and C21—H21*C*···O1^{v}, representing the growth characteristics of each crystal.

6. Molecular Docking Evaluation

One of the newest synthetic direct-acting compounds to be licensed for the treatment of therapeutic anticoagulation is Apixaban. To evaluate its potential as an anticoagulant agent, a molecular docking study of (I) as a ligand and the human coagulation factor hfXa as the receptor protein was performed. For the molecular coupling calculations, the free software *Autodock Vina 4.2.6* (Trott & Olson, 2010) was used, and as a positive control ligand in the active site, the molecule Apixaban (PDB code 2p16; Pinto *et al.*, 2007), one of the most important substrates currently accepted by the US Food and Drug Administration (FDA) for antithrombotic treatments (Agnelli *et al.*, 2013) was used. The Apixaban molecule was also used as a model for the validation and verification of the parameters of the molecular coupling calculations performed. The bonding energy obtained for the new inhibitor was −7.7 and −10.7 kcal mol^{-1} for the control ligand (Table 2). Compound (I), as a ligand at the active site of hfXa, presents one hydrogen bond of medium strength between the local N2 atom and the amino acid residue Gly218. However, all hydrophobic residue contacts of the latter in its more stable configuration are also present in the positive control ligand with the exception of Glu217. The results of the molecular coupling calculations show that ligand (I) has two equivalent energy configurations, poses 2 and 3 (see Table 3), which differ energetically from pose 1 by only 0.1 and 0.3 kcal mol^{-1}, respectively. Thus, pose 3 presents a better 3D conformational arrangement at the active site, this pose being much more similar to that of the control ligand (see Fig. 6). This behavior implies that two of the three hydrogen bonds presented by the control ligand in the active site Gly216 and Gln192, plus all hydrophobic contacts of ligand (I) in its pose 3, coincide with those presented by the control ligand. For this reason, the difference in binding energy between (I) and the control ligand at the active site is due to the chemical difference between the functional groups present in each structure. The molecular coupling images were generated using the programs *PyMOL* (Rigsby & Parker, 2016) and *Ligplot+* (Laskowski & Swindells, 2011).

7. Database survey

A search of the Cambridge Structural Database (CSD, version 5.41, November 2019 update; Groom *et al.*, 2016) using [3-(benzoyl-λ^2-azanyl)phenyl](phenyl-λ^2-azanyl)methanone as the main skeleton gave 76 hits. Seven structures containing the [3-(benzoyl-λ^2-azanyl)phenyl](phenyl-λ^2-azanyl)methanone framework with nitro and methoxy groups as substituents similar to the title compound were found, *viz.*, *N*-{3-[*N*′-(2-

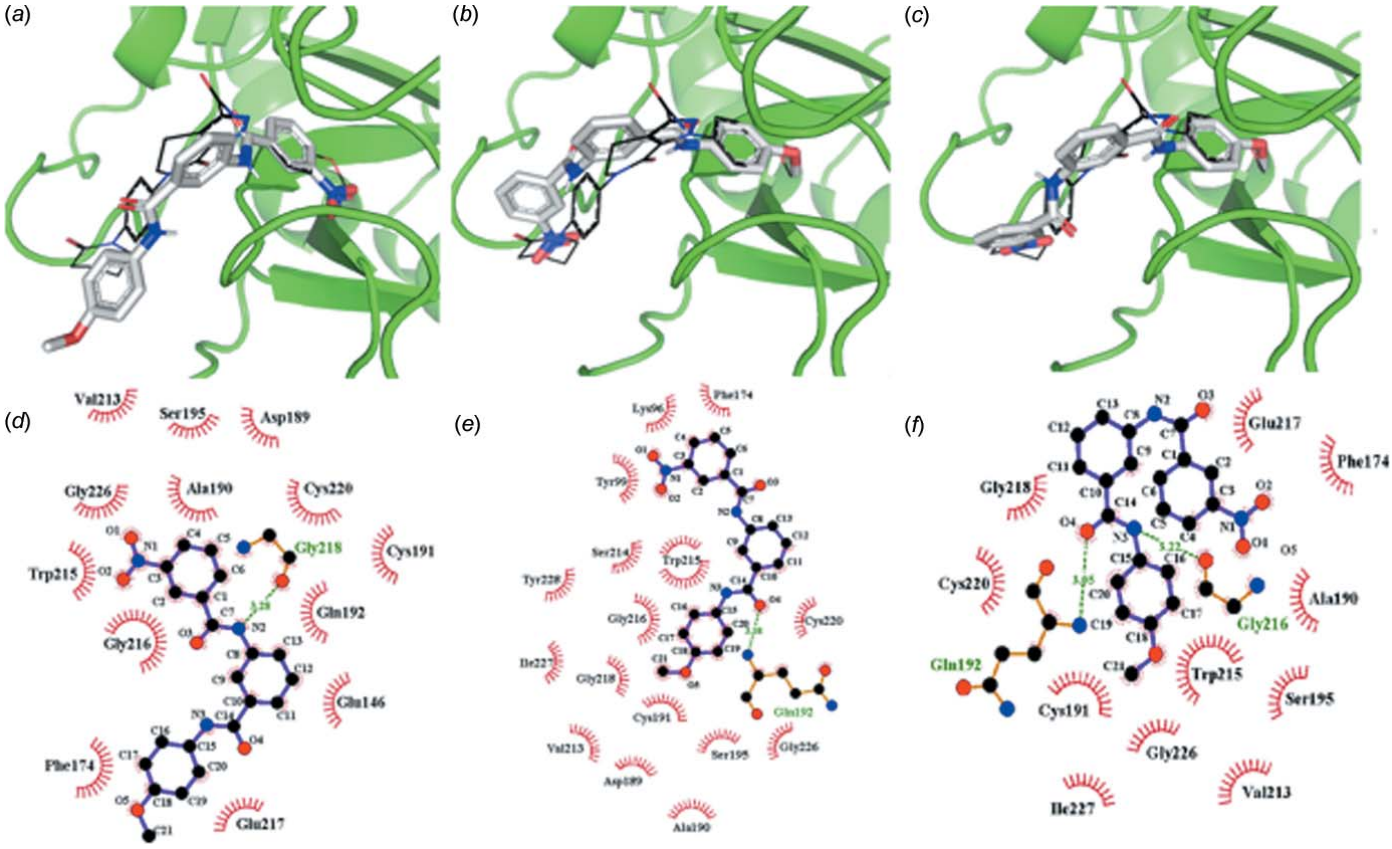

Figure 6
Models of molecular coupling for inhibition of hfXa by compound (I) in its poses: (*a*) and (*d*) pose 1; (*b*) and (*e*) pose 2, and (*c*) and (*f*) pose 3. Dashed lines indicate hydrogen bonds. Carbon atoms are in black, nitrogen in blue and oxygen in red.

methoxyphenyl)carbamoyl]-5-methyl-2-methoxyphenyl}-2-methoxy-5-methyl-3-nitrobenzamide (HEXXOY; Yi *et al.*, 2007), *N*-{3-[*N*′-(2-methoxyphenyl)carbamoyl]-5-methyl-2-methoxyphenyl}-2-hydroxy-5-methyl-3-nitrobenzamide (HEXYAL; Yi *et al.*, 2007), methyl 3-({2-hydroxy-3-[(2-methoxybenzoyl)amino]benzoyl}amino)-2-methoxybenzoate (POQMEP; Liu *et al.*, 2014), *catena*-[[μ-methyl 3-({2-oxy-3-[(2-methoxy-3-nitrobenzoyl)amino]benzoyl}amino)-2-methoxybenzoate]aquasodium methanol solvate] (POQMIT; Liu *et al.*, 2014), methyl 2-methoxy-3-({2-methoxy-3-[(2-methoxy-3-nitrobenzoyl)amino]benzoyl}amino)benzoate (YUXMIO; Yan *et al.*, 2010), methyl 3-({3-[(2,5-dimethoxy-3-nitrobenzoyl)amino]-2-methoxybenzoyl}amino)-2,5-dimethoxybenzoate (YUXNEL; Yan *et al.*, 2010), and methyl 3-({3-[(2,5-dimethoxy-3-nitrobenzoyl)amino]-2,5-dimethoxybenzoyl}amino)-2,5-dimethoxybenzoate (YUXNOV; Yan *et al.*, 2010). The specific characteristics of these diamide systems depend on the presence of the diverse substituents and their position in the rings in such a way that the planarity in the system is maintained between two rings and the third ring is rotated with respect to the first two. In this way, the compounds POQMEP, POQMIT and HEXXOY present a relatively small deviation from planarity, while the systems YUXNOV, YUXNEL, HEXYAL, YUXMIO progressively lose this planarity, ending up with quite large dihedral angles between the planes.

8. Synthesis and crystallization

3-Amino-*N*-(4-methoxyphenyl)benzamide (ii) (50.5 mg, 0.129 mmol), previously synthesized, was subjected to an acylation reaction in 3-nitrobenzoyl chloride (*a*) (50.5 mg, 0.272 mmol) under chloroform reflux conditions to obtain compound (I) [yield 44.7 mg (0.114 mmol), 88.4%; m.p. 502 (1) K].

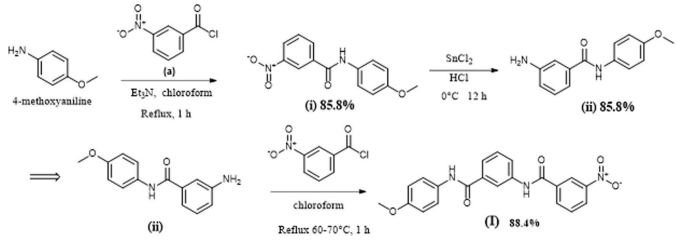

FT–IR (ATR): υ (cm^{-1}) = 3338, 3285 (N—H), 3076, 2969, 1650, 1637 (C═O), 1585 (C═C), 1526, 1510, 1434, 1353 (NO_2), 1316, 1301, 1241, 1137, 1026, 898, 829, 819, 721, 683 cm^{-1}. The UV–Vis spectrum for (I) (60 μM) was obtained in DMF with a maximum of 273 nm (0.62 absorption). MS (IE, 40 eV), m/z [M^+] calculated for $C_{21}H_{17}N_3O_5^+$: 391.12 (100%) and 392.12 (23.1%); found: 391.10 and 392.10 (25.1%).

9. Refinement

Crystal data, data collection and structure refinement details are summarized in Table 4. All the H atoms were found in a difference-Fourier map and were positioned at geometrically idealized positions, C—H = 0.95 Å (ring), N—H = 0.88 Å and C—H = 0.98 Å (methyl) and were refined using a riding-model approximation, with $U_{iso}(H) = 1.2U_{eq}$(parent atom) or $1.5U_{eq}(C)$. After refinement, ROTAX suggested twinning by a 180° about [100]. This law was used to generate an hklf5 format reflection file. Refinement against this file improved R factors and residual Q peaks·BASF refined to 0.090 (4)

Funding information

RMF is grateful to Universidad del Valle and Banco de la República Colombia for the support received for the realization of the CI 1169 project.

Table 4
Experimental details.

Crystal data	
Chemical formula	$C_{21}H_{17}N_3O_5$
M_r	391.37
Crystal system, space group	Monoclinic, $P2_1$
Temperature (K)	123
a, b, c (Å)	7.2948 (3), 7.1242 (3), 16.8297 (7)
β (°)	97.644 (3)
V (Å^3)	866.86 (6)
Z	2
Radiation type	Cu $K\alpha$
μ (mm^{-1})	0.91
Crystal size (mm)	0.50 × 0.40 × 0.18
Data collection	
Diffractometer	Oxford Diffraction Gemini S
Absorption correction	Multi-scan
T_{min}, T_{max}	0.603, 1.000
No. of measured, independent and observed [$I > 2\sigma(I)$] reflections	3172, 3172, 2982
R_{int}	0.048
$(\sin \theta/\lambda)_{max}$ (Å^{-1})	0.620
Refinement	
$R[F^2 > 2\sigma(F^2)]$, $wR(F^2)$, S	0.047, 0.126, 1.06
No. of reflections	3172
No. of parameters	263
No. of restraints	3
H-atom treatment	H-atom parameters constrained
$\Delta\rho_{max}$, $\Delta\rho_{min}$ (e Å^{-3})	0.23, −0.30
Absolute structure	Flack x determined using 524 quotients $[(I^+)-(I^-)]/[(I^+)+(I^-)]$ (Parsons *et al.*, 2013)
Absolute structure parameter	0.2 (3)

Computer programs: *CrysAlis PRO* (Agilent, 2014), *SIR92* (Altomare *et al.*, 1994), *SHELXL2014/7* (Sheldrick, 2015), *Mercury* (Macrae *et al.*, 2020) and *ORTEP-3 for Windows* (Farrugia, 2012).

References

Agilent (2014). *CrysAlis PRO*. Agilent Technologies Ltd, Yarnton, England.

Agnelli, G., Buller, H. R., Cohen, A., Curto, M., Gallus, A. S., Johnson, M., Porcari, A., Raskob, G. E. & Weitz, J. I. (2013). *N. Engl. J. Med.* **368**, 699–708.

Allen, F. H., Kennard, O., Watson, D. G., Brammer, L., Orpen, A. G. & Taylor, R. (1987). *J. Chem. Soc. Perkin Trans. 2*, pp. S1–S19.

Altomare, A., Cascarano, G., Giacovazzo, C., Guagliardi, A., Burla, M. C., Polidori, G. & Camalli, M. (1994). *J. Appl. Cryst.* **27**, 435.

Etter, M. C. (1990). *Acc. Chem. Res.* **23**, 120–126.

Farrugia, L. J. (2012). *J. Appl. Cryst.* **45**, 849–854.

Frisch, M. J., *et al.* (2009). *GAUSSIAN09*. Gaussian Inc., Wallingford, CT, USA.

Groom, C. R., Bruno, I. J., Lightfoot, M. P. & Ward, S. C. (2016). *Acta Cryst.* B**72**, 171–179.

Hathwar, V. R., Sist, M., Jørgensen, M. R. V., Mamakhel, A. H., Wang, X., Hoffmann, C. M., Sugimoto, K., Overgaard, J. & Iversen, B. B. (2015). *IUCrJ*, **2**, 563–574.

Hirata, Y., Sasaki, T., Kanki, H., Choong, C.-J., Nishiyama, K., Kubo, G., Hotei, A., Taniguchi, M. & Mochizuki, H. (2018). *Sci. Rep.* **8**, 1400, 1–9.

Lahm, G. P., Selby, T. P., Freudenberger, J. H., Stevenson, T. M., Myers, B. J., Seburyamo, G., Smith, B. K., Flexner, L., Clark, C. E. & Cordova, C. (2005). *Bioorg. Med. Chem. Lett.* **15**, 4898–4906.

Lahm, G. P., Stevenson, T. M., Selby, T. P., Freudenberger, J. H., Cordova, D., Flexner, L., Bellin, C. A., Dubas, C. M., Smith, B. K., Hughes, K. A., Hollingshaus, J. G., Clark, C. E. & Benner, E. A. (2007). *Bioorg. Med. Chem. Lett.* **17**, 6274–6279.

Laskowski, R. & Swindells, M. (2011). *J. Chem. Inf. Model.* **51**, 2778–2786.

Lee, S., Lee, W., Nguyen, T., Um, I., Bae, J. & Ma, E. (2017). *Int. J. Mol. Sci.* **18**, 1144–1170.

Liu, J., Sun, C., Ma, W., Lu, Y.-J., Yu, L., Zhang, K. & Zeng, H. (2014). *RSC Adv.* **4**, 54469–54473.

Lu, T. & Chen, F. (2012). *J. Mol. Graphics Modell.* **38**, 314–323.

Macrae, C. F., Sovago, I., Cottrell, S. J., Galek, P. T. A., McCabe, P., Pidcock, E., Platings, M., Shields, G. P., Stevens, J. S., Towler, M. & Wood, P. A. (2020). *J. Appl. Cryst.* **53**, 226–235.

Parsons, S., Flack, H. D. & Wagner, T. (2013). *Acta Cryst.* B**69**, 249–259.

Pinto, D., Orwat, M., Koch, S., Rossi, K., Alexander, R., Smallwood, A., Wong, P., Rendina, A., Luettgen, J., Knabb, R., He, K., Xin, B., Wexler, R. R. & Lam, P. Y. S. (2007). *J. Med. Chem.* **50**, 5339–5356.

Prasad, L. G., Krishnakumar, V., Nagalakshmi, R. & Manohar, S. (2011). *Mater. Chem. Phys.* **128**, 90–95.

Racagni, G., Canonico, P. L., Ravizza, L., Pani, L. & AMoRe, M. (2004). *Neuropsychobiology*, **50**, 134–143.

Rigsby, R. & Parker, A. (2016). *Biochem. Mol. Biol. Educ.* **44**, 433–437.

Sheldrick, G. M. (2015). *Acta Cryst.* C**71**, 3–8.

Spackman, M. A. & Jayatilaka, D. (2009). *CrystEngComm*, **11**, 19–32.

Tohnishi, M., Nakao, H., Furuya, T., Seo, A., Kodama, H., Tsubata, K., Fujioka, S., Kodama, H., Hirooka, T. & Nishimatsu, T. (2005). *J. Pestic. Sci.* **30**, 354–360.

Trott, O. & Olson, A. (2010). *J. Comput. Chem.* **31**, 455–461.

Turner, M. J., McKinnon, J. J., Wolff, S. K., Grimwood, D. J., Spackman, P. R., Jayatilaka, D. & Spackman, M. A. (2017). *CrystalExplorer17*. The University of Western Australia. http://https://crystalexplorer. scb. uwa. edu. au/.

Xing, J., Yang, L., Zhou, J. & Zhang, H. (2018). *Bioorg. Med. Chem.* **26**, 5987–5999.

Yan, Y., Qin, B., Ren, C., Chen, X., Yip, Y. K., Ye, R., Zhang, D., Su, H. & Zeng, H. (2010). *J. Am. Chem. Soc.* **132**, 5869–5879.

Yi, H.-P., Wu, J., Ding, K.-L., Jiang, X.-K. & Li, Z.-T. (2007). *J. Org. Chem.* **72**, 870–877.

supporting information

Acta Cryst. (2020). E**76**, 1762-1767 [https://doi.org/10.1107/S2056989020013730]

Synthesis, crystal structure, Hirshfeld surface analysis, MEP study and molecular docking of *N*-{3-[(4-methoxyphenyl)carbamoyl]phenyl}-3-nitrobenzamide as a promising inhibitor of hfXa

Rodolfo Moreno-Fuquen, Mario Hurtado-Angulo, Kevin Arango-Daraviña, Gavin Bain and Alan R. Kennedy

Computing details

Data collection: *CrysAlis PRO* (Agilent, 2014); cell refinement: *CrysAlis PRO* (Agilent, 2014); data reduction: *CrysAlis PRO* (Agilent, 2014); program(s) used to solve structure: *SIR92* (Altomare *et al.*, 1994); program(s) used to refine structure: *SHELXL2014/7* (Sheldrick, 2015); molecular graphics: *Mercury* (Macrae *et al.*, 2020); software used to prepare material for publication: *ORTEP-3 for Windows* (Farrugia, 2012).

N-{3-[(4-Methoxyphenyl)carbamoyl]phenyl}-3-nitrobenzamide

Crystal data

$C_{21}H_{17}N_3O_5$
M_r = 391.37
Monoclinic, $P2_1$
a = 7.2948 (3) Å
b = 7.1242 (3) Å
c = 16.8297 (7) Å
β = 97.644 (3)°
V = 866.86 (6) Å^3
Z = 2
F(000) = 408
D_x = 1.499 Mg m^{-3}
Melting point: 502(1) K
Cu $K\alpha$ radiation, λ = 1.54184 Å
Cell parameters from 3172 reflections
θ = 5.3–73.1°
μ = 0.91 mm^{-1}
T = 123 K
Fragment cut from large slab, pale yellow
0.50 × 0.40 × 0.18 mm

Data collection

Oxford Diffraction Gemini S diffractometer
Radiation source: sealed tube
ω scans
Absorption correction: multi-scan
T_{min} = 0.603, T_{max} = 1.000
3172 measured reflections
3172 independent reflections
2982 reflections with $I > 2\sigma(I)$
R_{int} = 0.048
θ_{max} = 73.1°, θ_{min} = 5.3°
$h = -8 \rightarrow 6$
$k = -8 \rightarrow 8$
$l = -20 \rightarrow 20$

Refinement

Refinement on F^2
Least-squares matrix: full
$R[F^2 > 2\sigma(F^2)]$ = 0.047
$wR(F^2)$ = 0.126
S = 1.06
3172 reflections
263 parameters
3 restraints
Hydrogen site location: inferred from neighbouring sites
H-atom parameters constrained
$w = 1/[\sigma^2(F_o^2) + (0.066P)^2 + 0.3205P]$ where $P = (F_o^2 + 2F_c^2)/3$
$(\Delta/\sigma)_{max}$ < 0.001

$\Delta\rho_{max}$ = 0.23 e Å^{-3}
$\Delta\rho_{min}$ = −0.30 e Å^{-3}

Absolute structure: Flack *x* determined using 524 quotients [(I^+)-(I^-)]/[(I^+)+(I^-)] (Parsons *et al.*, 2013)
Absolute structure parameter: 0.2 (3)

Special details

Experimental. CrysAlisPro, Agilent Technologies, Version 1.171.37.35 (release 13-08-2014 CrysAlis171 .NET) (compiled Aug 13 2014,18:06:01) Empirical absorption correction using spherical harmonics, implemented in SCALE3 ABSPACK scaling algorithm.

Geometry. All esds (except the esd in the dihedral angle between two l.s. planes) are estimated using the full covariance matrix. The cell esds are taken into account individually in the estimation of esds in distances, angles and torsion angles; correlations between esds in cell parameters are only used when they are defined by crystal symmetry. An approximate (isotropic) treatment of cell esds is used for estimating esds involving l.s. planes.

Refinement. Refined as a two-component twin
After refinement ROTAX suggested twinning by a 180 rotation about direct 1 0 0.
This law was used to generate a hklf5 formated reflection file.
Refinement against this file improved R factors and residual Q peaks.
BASF refined to 0.090 (4)

Fractional atomic coordinates and isotropic or equivalent isotropic displacement parameters (Å²)

	x	*y*	*z*	U_{iso}*/U_{eq}
O1	0.6697 (5)	0.7564 (5)	0.02367 (18)	0.0376 (8)
O2	0.5804 (5)	0.9765 (5)	0.09701 (19)	0.0350 (7)
O3	0.2455 (4)	0.5231 (5)	0.35551 (16)	0.0282 (6)
O4	0.2775 (4)	0.5306 (4)	0.64175 (16)	0.0263 (6)
O5	−0.1675 (4)	0.3265 (4)	0.93736 (17)	0.0277 (7)
N1	0.6116 (4)	0.8119 (5)	0.0852 (2)	0.0246 (7)
N2	0.3987 (4)	0.8014 (5)	0.37262 (18)	0.0197 (7)
H2N	0.4792	0.8744	0.3531	0.024*
N3	0.0451 (4)	0.7137 (5)	0.67641 (19)	0.0198 (7)
H3N	−0.0181	0.8174	0.6646	0.024*
C1	0.4599 (5)	0.5945 (6)	0.2656 (2)	0.0200 (8)
C2	0.5006 (5)	0.7309 (6)	0.2117 (2)	0.0201 (7)
H2	0.4757	0.8598	0.2199	0.024*
C3	0.5793 (5)	0.6713 (6)	0.1453 (2)	0.0214 (8)
C4	0.6237 (5)	0.4862 (7)	0.1322 (2)	0.0249 (8)
H4	0.6775	0.4510	0.0860	0.030*
C5	0.5880 (5)	0.3544 (6)	0.1879 (2)	0.0263 (9)
H5	0.6220	0.2271	0.1817	0.032*
C6	0.5021 (5)	0.4077 (6)	0.2532 (2)	0.0223 (8)
H6	0.4718	0.3150	0.2899	0.027*
C7	0.3569 (5)	0.6363 (6)	0.3358 (2)	0.0212 (8)
C8	0.3212 (5)	0.8658 (6)	0.4411 (2)	0.0187 (8)
C9	0.2817 (5)	0.7434 (6)	0.5012 (2)	0.0186 (7)
H9	0.3051	0.6129	0.4968	0.022*
C10	0.2080 (5)	0.8120 (6)	0.5675 (2)	0.0190 (8)
C11	0.1753 (5)	1.0041 (6)	0.5751 (2)	0.0207 (8)
H11	0.1239	1.0508	0.6202	0.025*
C12	0.2191 (5)	1.1265 (6)	0.5156 (2)	0.0229 (8)

H12	0.1986	1.2574	0.5207	0.028*
C13	0.2922 (5)	1.0588 (6)	0.4492 (2)	0.0213 (8)
H13	0.3225	1.1433	0.4093	0.026*
C14	0.1800 (5)	0.6713 (6)	0.6309 (2)	0.0199 (8)
C15	−0.0029 (5)	0.6049 (6)	0.7415 (2)	0.0185 (8)
C16	0.0253 (5)	0.4121 (6)	0.7483 (2)	0.0217 (8)
H16	0.0805	0.3463	0.7085	0.026*
C17	−0.0274 (5)	0.3165 (6)	0.8134 (2)	0.0217 (8)
H17	−0.0067	0.1850	0.8181	0.026*
C18	−0.1096 (5)	0.4096 (6)	0.8715 (2)	0.0218 (8)
C19	−0.1431 (6)	0.6016 (6)	0.8636 (2)	0.0249 (9)
H19	−0.2038	0.6659	0.9021	0.030*
C20	−0.0880 (5)	0.6982 (6)	0.7997 (2)	0.0236 (9)
H20	−0.1082	0.8297	0.7954	0.028*
C21	−0.1360 (6)	0.1300 (7)	0.9478 (3)	0.0312 (10)
H21A	−0.1834	0.0882	0.9967	0.047*
H21B	−0.2001	0.0623	0.9015	0.047*
H21C	−0.0031	0.1045	0.9524	0.047*

Atomic displacement parameters (Å²)

	U^{11}	U^{22}	U^{33}	U^{12}	U^{13}	U^{23}
O1	0.0561 (19)	0.0329 (18)	0.0277 (15)	0.0003 (16)	0.0204 (14)	−0.0033 (15)
O2	0.0502 (18)	0.0226 (18)	0.0357 (17)	−0.0006 (14)	0.0189 (14)	0.0045 (14)
O3	0.0308 (14)	0.0276 (16)	0.0280 (14)	−0.0096 (14)	0.0108 (11)	−0.0054 (13)
O4	0.0270 (13)	0.0223 (15)	0.0321 (14)	0.0074 (12)	0.0132 (11)	0.0065 (13)
O5	0.0359 (15)	0.0235 (16)	0.0254 (14)	−0.0018 (13)	0.0099 (11)	0.0038 (13)
N1	0.0271 (16)	0.0230 (19)	0.0244 (17)	−0.0037 (14)	0.0065 (13)	−0.0036 (15)
N2	0.0203 (14)	0.0194 (17)	0.0210 (14)	−0.0040 (12)	0.0087 (11)	0.0000 (13)
N3	0.0208 (14)	0.0169 (16)	0.0221 (15)	0.0033 (13)	0.0043 (11)	0.0014 (13)
C1	0.0181 (16)	0.023 (2)	0.0190 (17)	−0.0018 (15)	0.0037 (13)	−0.0007 (16)
C2	0.0188 (16)	0.0200 (19)	0.0216 (17)	−0.0012 (15)	0.0027 (13)	−0.0014 (16)
C3	0.0216 (17)	0.021 (2)	0.0215 (18)	−0.0018 (15)	0.0030 (14)	−0.0031 (16)
C4	0.0231 (17)	0.027 (2)	0.0251 (18)	−0.0018 (16)	0.0046 (14)	−0.0064 (18)
C5	0.026 (2)	0.019 (2)	0.034 (2)	0.0037 (16)	0.0035 (16)	−0.0049 (17)
C6	0.0236 (18)	0.017 (2)	0.0263 (19)	−0.0004 (15)	0.0021 (14)	0.0023 (17)
C7	0.0186 (16)	0.023 (2)	0.0218 (17)	0.0017 (16)	0.0039 (13)	0.0038 (16)
C8	0.0151 (16)	0.021 (2)	0.0202 (17)	−0.0026 (14)	0.0022 (13)	−0.0001 (16)
C9	0.0188 (15)	0.0165 (19)	0.0213 (18)	−0.0012 (14)	0.0053 (13)	−0.0019 (16)
C10	0.0156 (15)	0.0189 (19)	0.0227 (18)	−0.0002 (15)	0.0030 (13)	−0.0011 (17)
C11	0.0197 (16)	0.021 (2)	0.0227 (17)	0.0001 (16)	0.0061 (13)	−0.0013 (17)
C12	0.0227 (17)	0.0156 (19)	0.030 (2)	0.0000 (15)	0.0027 (15)	−0.0003 (17)
C13	0.0207 (16)	0.019 (2)	0.0239 (18)	−0.0027 (15)	0.0038 (14)	0.0058 (16)
C14	0.0181 (16)	0.0194 (19)	0.0219 (18)	−0.0013 (15)	0.0018 (13)	−0.0022 (16)
C15	0.0164 (15)	0.020 (2)	0.0189 (17)	−0.0005 (14)	0.0023 (13)	−0.0014 (16)
C16	0.0226 (18)	0.019 (2)	0.0244 (19)	0.0015 (16)	0.0065 (15)	−0.0033 (17)
C17	0.0225 (17)	0.0146 (19)	0.0282 (19)	−0.0001 (15)	0.0045 (14)	0.0008 (17)
C18	0.0202 (17)	0.024 (2)	0.0211 (17)	−0.0045 (15)	0.0015 (14)	0.0017 (17)

C19	0.0290 (19)	0.024 (2)	0.0235 (18)	0.0011 (16)	0.0090 (15)	−0.0035 (17)
C20	0.0258 (18)	0.021 (2)	0.0245 (19)	0.0027 (16)	0.0061 (15)	0.0013 (17)
C21	0.031 (2)	0.030 (2)	0.033 (2)	−0.0023 (19)	0.0060 (17)	0.012 (2)

Geometric parameters (Å, º)

O1—N1	1.235 (5)	C8—C9	1.394 (5)
O2—N1	1.216 (5)	C8—C13	1.401 (6)
O3—C7	1.221 (5)	C9—C10	1.390 (5)
O4—C14	1.229 (5)	C9—H9	0.9500
O5—C18	1.372 (5)	C10—C11	1.398 (6)
O5—C21	1.425 (5)	C10—C14	1.498 (5)
N1—C3	1.465 (5)	C11—C12	1.396 (6)
N2—C7	1.346 (5)	C11—H11	0.9500
N2—C8	1.425 (5)	C12—C13	1.388 (5)
N2—H2N	0.8800	C12—H12	0.9500
N3—C14	1.359 (5)	C13—H13	0.9500
N3—C15	1.424 (5)	C15—C16	1.391 (5)
N3—H3N	0.8800	C15—C20	1.396 (5)
C1—C2	1.388 (6)	C16—C17	1.388 (6)
C1—C6	1.389 (6)	C16—H16	0.9500
C1—C7	1.511 (5)	C17—C18	1.383 (6)
C2—C3	1.389 (5)	C17—H17	0.9500
C2—H2	0.9500	C18—C19	1.392 (6)
C3—C4	1.383 (6)	C19—C20	1.380 (6)
C4—C5	1.376 (6)	C19—H19	0.9500
C4—H4	0.9500	C20—H20	0.9500
C5—C6	1.389 (6)	C21—H21A	0.9800
C5—H5	0.9500	C21—H21B	0.9800
C6—H6	0.9500	C21—H21C	0.9800
C18—O5—C21	117.5 (3)	C9—C10—C14	116.1 (4)
O2—N1—O1	122.6 (4)	C11—C10—C14	123.2 (4)
O2—N1—C3	119.7 (3)	C12—C11—C10	119.2 (4)
O1—N1—C3	117.7 (4)	C12—C11—H11	120.4
C7—N2—C8	124.3 (3)	C10—C11—H11	120.4
C7—N2—H2N	117.8	C13—C12—C11	120.6 (4)
C8—N2—H2N	117.8	C13—C12—H12	119.7
C14—N3—C15	125.8 (3)	C11—C12—H12	119.7
C14—N3—H3N	117.1	C12—C13—C8	119.9 (4)
C15—N3—H3N	117.1	C12—C13—H13	120.0
C2—C1—C6	120.1 (4)	C8—C13—H13	120.0
C2—C1—C7	123.0 (4)	O4—C14—N3	123.0 (4)
C6—C1—C7	116.7 (4)	O4—C14—C10	121.4 (3)
C1—C2—C3	117.3 (4)	N3—C14—C10	115.5 (4)
C1—C2—H2	121.3	C16—C15—C20	119.2 (4)
C3—C2—H2	121.3	C16—C15—N3	123.4 (4)
C4—C3—C2	123.4 (4)	C20—C15—N3	117.4 (3)

C4—C3—N1	118.6 (4)	C17—C16—C15	119.7 (4)
C2—C3—N1	117.9 (4)	C17—C16—H16	120.2
C5—C4—C3	118.2 (4)	C15—C16—H16	120.2
C5—C4—H4	120.9	C18—C17—C16	121.0 (4)
C3—C4—H4	120.9	C18—C17—H17	119.5
C4—C5—C6	120.0 (4)	C16—C17—H17	119.5
C4—C5—H5	120.0	O5—C18—C17	124.9 (4)
C6—C5—H5	120.0	O5—C18—C19	115.6 (4)
C5—C6—C1	120.9 (4)	C17—C18—C19	119.4 (4)
C5—C6—H6	119.5	C20—C19—C18	119.9 (4)
C1—C6—H6	119.5	C20—C19—H19	120.0
O3—C7—N2	124.7 (4)	C18—C19—H19	120.0
O3—C7—C1	120.0 (4)	C19—C20—C15	120.8 (4)
N2—C7—C1	115.2 (3)	C19—C20—H20	119.6
C9—C8—C13	119.7 (3)	C15—C20—H20	119.6
C9—C8—N2	121.8 (4)	O5—C21—H21A	109.5
C13—C8—N2	118.4 (4)	O5—C21—H21B	109.5
C10—C9—C8	120.1 (4)	H21A—C21—H21B	109.5
C10—C9—H9	119.9	O5—C21—H21C	109.5
C8—C9—H9	119.9	H21A—C21—H21C	109.5
C9—C10—C11	120.5 (4)	H21B—C21—H21C	109.5

C6—C1—C2—C3	1.6 (5)	C9—C10—C11—C12	−0.6 (5)
C7—C1—C2—C3	−173.7 (3)	C14—C10—C11—C12	175.0 (3)
C1—C2—C3—C4	−2.2 (5)	C10—C11—C12—C13	0.7 (6)
C1—C2—C3—N1	175.9 (3)	C11—C12—C13—C8	0.5 (6)
O2—N1—C3—C4	−177.1 (4)	C9—C8—C13—C12	−2.0 (6)
O1—N1—C3—C4	3.1 (5)	N2—C8—C13—C12	−179.2 (3)
O2—N1—C3—C2	4.7 (5)	C15—N3—C14—O4	−0.2 (6)
O1—N1—C3—C2	−175.2 (3)	C15—N3—C14—C10	−178.0 (3)
C2—C3—C4—C5	0.0 (6)	C9—C10—C14—O4	28.3 (5)
N1—C3—C4—C5	−178.1 (3)	C11—C10—C14—O4	−147.5 (4)
C3—C4—C5—C6	2.8 (6)	C9—C10—C14—N3	−153.8 (3)
C4—C5—C6—C1	−3.3 (6)	C11—C10—C14—N3	30.4 (5)
C2—C1—C6—C5	1.1 (6)	C14—N3—C15—C16	−26.6 (6)
C7—C1—C6—C5	176.7 (3)	C14—N3—C15—C20	155.5 (4)
C8—N2—C7—O3	1.3 (6)	C20—C15—C16—C17	−1.4 (6)
C8—N2—C7—C1	−178.4 (3)	N3—C15—C16—C17	−179.3 (3)
C2—C1—C7—O3	142.4 (4)	C15—C16—C17—C18	0.7 (6)
C6—C1—C7—O3	−33.1 (5)	C21—O5—C18—C17	1.8 (6)
C2—C1—C7—N2	−37.9 (5)	C21—O5—C18—C19	180.0 (4)
C6—C1—C7—N2	146.6 (3)	C16—C17—C18—O5	179.4 (3)
C7—N2—C8—C9	36.2 (5)	C16—C17—C18—C19	1.3 (6)
C7—N2—C8—C13	−146.6 (4)	O5—C18—C19—C20	179.3 (3)
C13—C8—C9—C10	2.1 (5)	C17—C18—C19—C20	−2.4 (6)
N2—C8—C9—C10	179.3 (3)	C18—C19—C20—C15	1.7 (6)
C8—C9—C10—C11	−0.9 (5)	C16—C15—C20—C19	0.3 (6)
C8—C9—C10—C14	−176.8 (3)	N3—C15—C20—C19	178.3 (4)

Hydrogen-bond geometry (Å, º)

D—H···*A*	*D*—H	H···*A*	*D*···*A*	*D*—H···*A*
N2—H2*N*···O4^{i}	0.88	2.09	2.908 (4)	155
N3—H3*N*···O3^{ii}	0.88	2.21	3.056 (4)	163
C5—H5···O2^{iii}	0.95	2.28	3.093 (5)	143
C19—H19···O1^{iv}	0.95	2.44	3.365 (5)	164
C21—H21*C*···O1^{v}	0.98	2.64	3.490 (5)	145

Symmetry codes: (i) −*x*+1, *y*+1/2, −*z*+1; (ii) −*x*, *y*+1/2, −*z*+1; (iii) *x*, *y*−1, *z*; (iv) *x*−1, *y*, *z*+1; (v) −*x*+1, *y*−1/2, −*z*+1.